Carbohydrate Polymers 110 (2014) 440–445

Contents lists available at ScienceDirect

Carbohydrate Polymers

journal homepage: www.elsevier.com/locate/carbpol

Thermoresponsive magnetic nanoparticle – Aminated guar gum hydrogel system for sustained release of doxorubicin hydrochloride

Ragothaman Murali, Ponraj Vidhya, Palanisamy Thanikaivelan*

Advanced Materials Laboratory, Centre for Leather Apparel & Accessories Development, Central Leather Research Institute (Council of Scientific and Industrial Research), Adyar, Chennai 600020, India

ARTICLE INFO

Article history:
Received 24 January 2014
Received in revised form 24 March 2014
Accepted 15 April 2014
Available online 26 April 2014

Keywords:
Solid tumor
Biomedical imaging
Aminated guar gum
Core–shell nanoparticles
Doxorubicin HCl

ABSTRACT

Hydrogel based sustained drug delivery system has evolved as an immense treatment method for solid tumors over the past few decades with long term theranostic ability. Here, we synthesized an injectable hydrogel system comprising biocompatible aminated guar gum, Fe_3O_4–ZnS core–shell nanoparticles and doxorubicin hydrochloride. We show that amination of guar gum resulted in attraction of water molecules thereby forming the hydrogel without using toxic crosslinking agents. Hydrogel formation was observed at 37 °C and is stable up to 95 °C. The prepared hydrogel is also stable over a wide pH range. The in vitro studies show that the maximum de-gelation and drug release up to 90% can be achieved after 20 days of incubation. Studies reveal that the drug and the core–shell nanoparticles can be released slowly from the hydrogel to provide the healing and diagnosis of the solid tumor thereby avoiding several drug administrations and total excision of organs.

1. Introduction

Direct administration of chemotherapeutic agents in cancerous solid tumors has shown severe side effects in the system (Kintzel & Dorr, 1995). Injectable hydrogel is an alternative and effective system that can deliver the drug to specific tissues thereby reducing the drug side effects as well as the injection frequency (Arola et al., 2000; Kim et al., 2012). Currently, injectable hydrogel system comprising both therapeutic and diagnostic imaging agents is an emerging research area for effective guided therapy (Kim et al., 2012). Guar gum (GG) is one of the high-molecular weight, water-soluble, non-ionic biopolymer derived from the endosperm of guar beans, which has been widely used in the pharmaceuticals products primarily due to its unique ability to alter rheological properties (Burke, Park, Srinivasarao, & Khan, 2000). Several studies have been carried out to increase the mechanical, thermal and viscosity properties of the GG by chemical modification (Bajpai, Saxena, & Sharma, 2006; Huang, Lu, & Xiao, 2007). The chemically modified GG cross-linked with glutaraldehyde, phosphate, urea-formaldehyde or borax has been used for various applications such as controlled drug release (Soppirnath & Aminabhavi, 2002), colon-specific drug delivery (Chourasia & Jain, 2004; Gliko-Kabir, Yagen, Baluom, & Rubinstein, 2000), liquid pesticide (Kulkarni, Soppimath, Aminabhavi, Dave, & Mehta, 1999), water retention (Tayal, Pai, & Khan, 1999), synthetic cervical mucus (Burruano, Schnaare, & Malamud, 2002) and transdermal drug delivery systems (Narasimha Murthy, Hiremath, & Paranjothy, 2004) due to its high biocompatibility and biodegradability. However, the preparation of chemically cross-linked hydrogel using toxic crosslinkers poses significant limitations in the applications (Chang & Zhang, 2011).

Inclusion of magnetic resonance imaging (MRI) agents in the injectable hydrogel helps in depiction of targeted agent and diagnosis of the lesion sites. Iron oxide nanoparticles (IONP) are prominently used as MRI agent for biological applications (Corot, Robert, Idee, & Port, 2006). A suitable chemical modification has been indispensable for the IONP, which has intended to reduce the alteration of magnetic properties, agglomeration and rapid degradation (Kim et al., 2012; Santra et al., 2001). It has been used clinically for various biomedical applications, such as hyperthermia, drug delivery, tissue repair, cell and tissue targeting and transfection (Gupta & Gupta, 2005; Gupta, Naregalkar, Vaidya, & Gupta, 2007). Doxorubicin hydrochloride (DOX) is one of the most widely used chemotherapeutic anticancer drugs, however, it initiates serious side effects such as cardiotoxicity, bone marrow and gastrointestinal toxicity if applied directly (Arola et al., 2000; Von Hoff et al., 1979). Several studies reveal that the encapsulated DOX reduces the toxicity and side effects of the drug (Gelperina et al., 2002; Yoo, Lee, Oh, & Park, 2000). It has been shown that the conjugation of DOX with the dextran and liposomes not only

* Corresponding author. Tel.: +91 44 24910953; fax: +91 44 24910953.
E-mail addresses: thanik8@yahoo.com, thanik8@gmail.com (P. Thanikaivelan).

http://dx.doi.org/10.1016/j.carbpol.2014.04.076
0144-8617/

reduces the cytotoxicity but also enhances the efficiency of the drug (Mitra, Gaur, Ghosh, & Maitra, 2001; Wong et al., 2006). Here, an approach has been made to prepare aminated guar gum (AGG) from GG by reacting with ethylene diamine and sodium borohydride (Simi & Abraham, 2010). The reaction leads to the substitution of —OH group with $-NH_2$ group at the 2nd, 3rd, and 6th position in the monosaccharide units of polysaccharide backbones. We also report a simple approach to prepare injectable hydrogel system using the AGG incorporated with iron oxide–zinc sulphide core–shell nanoparticles (CSNP) and DOX, which could eliminate the limitations such as instability and cytotoxicity. The prepared AGG, IONP, CSNP and injectable hydrogel systems were investigated for the chemical, structural, magnetic and biological properties.

2. Materials and methods

2.1. Materials

Ferric chloride ($FeCl_3$) was purchased from M/s SD Fine-Chem, Mumbai, India. Ferrous sulphate ($FeSO_4{\cdot}7H_2O$) and acetone were purchased from Merck, Mumbai, India. Ammonium hydroxide (25%) was procured from M/s Sisco Research Lab, Mumbai, India. Zinc acetate ($Zn(CH_3COO)_2$), sodium borohydride ($NaBH_4$) and guar gum powder were procured from Himedia, India. Ethylene diamine ($C_2H_8N_2$), sodium sulfide (Na_2S) and doxorubicin HCl were purchased from Sigma–Aldrich Chemicals. All other reagents were of analytical grade.

2.2. Synthesis of aminated guar gum

The synthesis of AGG was carried out by the addition of $C_2H_8N_2$ as an aminating agent to the GG, which substituted the —OH group of the GG with $-NHCH_2CH_2NH_2$. Further the $-NHCH_2CH_2NH_2$ group was reduced to $-NH_2$ group by the addition of $NaBH_4$ (Simi & Abraham, 2010). 1 g (w/v) of GG was dissolved in 250 ml of distilled water and stirred to get homogenous solution for 30 min. 25 ml of ethylene diamine was added to the homogenous solution of GG and allowed to react with continuous stirring for overnight at room temperature. Then, 50 ml of 5% $NaBH_4$ solution was added to the reaction mixture and stirred vigorously for 3 h. After the completion of the reaction, the mixture was precipitated and washed several times with acetone. The precipitated sample was lyophilized and then powdered to uniform particles.

2.3. Synthesis of core–shell nanoparticles

The synthesis of CSNP was carried out in two steps. In the first step, iron oxide nanoparticles were synthesized. In the typical Fe_3O_4 nanoparticles synthesis, 20 ml of 0.1 M $FeCl_3$ and 20 ml of 0.05 M $FeSO_4$ were mixed and stirred for 30 min at room temperature. To this solution, NH_4OH was added drop wise to attain pH 10. A black color precipitate was formed signifying the formation of Fe_3O_4 nanoparticles. The precipitate was washed repeatedly with acetone and dried at 55 °C. In the second step, the Fe_3O_4 nanoparticles (10 ml, 0.1%, w/v) were sonicated to remove the agglomeration for 30 min at 30 ± 2 °C. After sonication, Na_2S (5 ml, 0.15 M) was added and stirred continuously for 30 min to facilitate deposition of sulphide ions on the surface of Fe_3O_4 nanoparticles. Then, 10 ml of 0.3 M $Zn(CH_3COO)_2$ was added to the solution and stirred for 3 h. The precipitated CSNP were washed with acetone several times. The collected precipitate was dried at 55 °C and then ground to make fine powder.

2.4. Characterization

The amino group in the AGG was determined by 2,4,6-trinitrobenzenesulfonic acid (TNBS) assay (Bubnis & Ofner, 1992). It is known that the TNBS reacts with amines, hydrazines and hydrazides groups to form a stable trinitrophenyl complex. Briefly, 5 mg of samples from GG and AGG were dissolved in 1 ml of distilled water. To this solution, 1 ml of 4% (w/v) $NaHCO_3$ and 1 ml of freshly prepared 0.5% (v/v) TNBS solution were added and kept at 60 °C for 4 h. After that, 1 ml of the reacted solution was transferred to a fresh test tube and mixed with 3 ml of 6 M HCl. The tubes were kept at 40 °C for 1.5 h and the absorbance of formed trinitrophenyl complex was measured using UV–visible spectrophotometer (Schimadzu, UV-1800) at 420 nm. The percentage of amino group substituted in the GG was calculated using the equation below:

$$\text{degree of substitution}\,(\%) = \frac{\text{AGG absorbance value} - \text{GG absorbance value}}{\text{AGG absorbance value}} \times 100$$

The GG, AGG, IONP and CSNP were analyzed using Perkin Elmer FT-IR spectrometer. The samples were ground with KBr and compressed to form pellets. The pellets were analyzed in a single beam mode at the range of 400–4000 cm^{-1} with an average of 4 scans and 2 cm^{-1} resolution. X-ray diffraction was performed to identify the crystallographic structure of IONP and CSNP by using Rigaku Miniflex (II) desktop diffractometer (Ni filtered CuK_α radiation with $\lambda = 0.15418$ nm). The samples were analyzed in the 2θ range of 10–80° in a step of 0.02° and with a counting time of 10 s per step. Elemental composition of IONP and CSNP was investigated through energy dispersive X-ray analysis (EDX) using Oxford Instruments NanoAnalysis (INCA Energy 250 Microanalysis System). The magnetic properties of the synthesized IONP and CSNP were measured using the vibrating sample magnetometer (VSM, Lakeshore, 7410 model) at room temperature. The morphology, size and structure of the IONP and CSNP nanoparticles were analyzed using high resolution – scanning electron microscopy (HRSEM, Quanta 200 series, FEI Company) and high resolution – transmission electron microscopy (HRTEM, JEOL 3010).

2.5. Preparation of injectable hydrogel

The injectable AGG-CSNP-DOX hydrogel (100/0.125/0.05 wt.%) was prepared by the following method as shown in Fig. 1. Initially, 25 ml of 0.01% (w/v) solution of CSNP was sonicated for 30 min at 30 ± 2 °C. After the complete dispersion, the AGG (2 g) and DOX (1 ml, 0.1%, w/v) were added to the solution. These solutions were uniformly dispersed by sonication at 37 °C for 15 min to form stable injectable AGG-CSNP-DOX (100/0.125/0.05 wt.%) hydrogel. Likewise, the AGG (100 wt.%) and AGG-CSNP (100/0.125 wt.%) hydrogels were prepared by using the respective dispersed compositions as above.

2.6. Effect of temperature and pH on the hydrogel

The effect of different temperature and pH conditions on the as-synthesized AGG, AGG-CSNP and AGG-CSNP-DOX hydrogel systems were studied. For studying the effect of temperature (0–95 °C) on the hydrogel systems, temperature controlled heating water bath and ice bath were employed. For studying the effect of pH (2–12) on the hydrogel systems, 1 M NaOH and 1 M HCl solutions were employed.

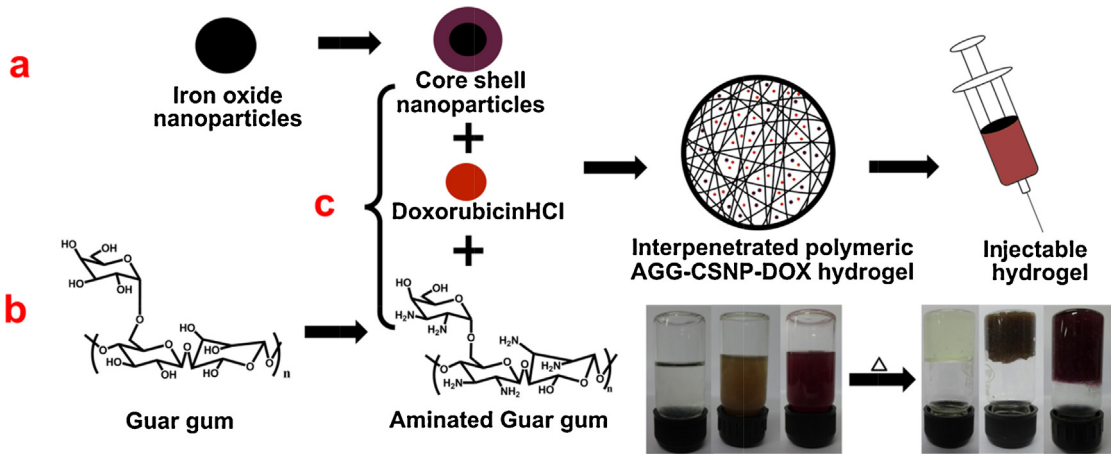

Fig. 1. Schematic showing (a) the synthesis of CSNP from IONP, (b) the synthesis of AGG from GG and (c) the preparation of AGG-CSNP-DOX injectable hydrogel system.

2.7. In vitro de-gelation studies

The in vitro de-gelation of the AGG, AGG-CSNP and AGG-CSNP-DOX hydrogel systems was carried out by incubating a known weight of hydrogel into the 25 ml of phosphate buffered saline (PBS) solution (pH 7.4) at 37 °C. The weight of in vitro de-gelated hydrogels was measured after removal of surface water using filter paper at different time periods. The percentage de-gelation was calculated by using the equation below:

$$\text{in vitro degelation}\,(\%) = \frac{\text{initial weight} - \text{final weight}}{\text{initial weight}} \times 100$$

2.8. In vitro drug release study

The in vitro drug release tendency was studied by incubating the AGG-CSNP-DOX injectable hydrogel into 25 ml PBS (pH 7.4) solution at 37 °C. The amount of DOX released from the encapsulated hydrogel was determined at different time periods using UV-visible spectrophotometer at 486 nm. The cumulative DOX release from the injectable hydrogel was calculated using the equation below:

$$\text{in vitro drug release}\,(\%) = \frac{\text{amount of DOX released}}{\text{initial amount of DOX}} \times 100$$

3. Results and discussion

3.1. Degree of substitution

The AGG was prepared by reacting $C_2H_8N_2$ and $NaBH_4$ with the GG. It is seen that the degree of substitution of amino group in guar gum is up to 61% as analyzed through the TNBS method. The results clearly indicate the presence of NH_2 group in AGG and confirm the modification of GG. The presence of amino group in the GG biopolymer attracts water molecules thereby leading to the formation of hydrogel. The amination process expected to create ionic imbalances in the biopolymer due to the formation of NH_3^+ (Simi & Abraham, 2010). We propose that the cationic charge attracts more water molecules in order to neutralize the system by forming AGG-$NH_3^+ - {}^-(\delta^-(OH^- - H^+))_n$ hydrogel. Each water molecule provides a partial negative charge (δ^-) such that several water molecules can cumulatively satisfy and neutralize one positive charge of the AGG. Therefore, AGG with several cationic amino groups would require more number of water molecules to neutralize several positive charges thereby forming the hydrogel.

3.2. FTIR analysis

The FTIR spectrum of pure GG, AGG, IONP and CSNP are shown in Fig. 2. The FT-IR spectrum of pure GG depicts a broad absorption band at 3352 cm^{-1}, which indicates the presence of significant quantity of hydroxyl groups in the structure (Fig. 2a). In the modified GG (Fig. 2b), this band became sharper and shifted from 3352 to 3423 cm^{-1} due to the substitution of $-NH_2$ functional group to the —OH group in the structure (Simi & Abraham, 2010). Further, the AGG shows appearance of a sharp peak around 1030 cm^{-1}, which corresponds to C—N stretching vibration of aliphatic amine. Hence, these results are in agreement with the amino group determination study of the AGG.

FT-IR spectrum of IONP exhibits major bands at 1740, 1628, 1401, 1123, 1051, 593 and 460 cm^{-1} (Fig. 2c). The band at 1628 cm^{-1} corresponds to hydroxyl group of moisture while the bands at 1740, 1401, 1123 and 1051 cm^{-1} correspond to C—O vibration arising from the presence of CO_2 from air. The characteristic peaks seen at 593 and 460 cm^{-1} correspond to the Fe—O stretching vibration of the IONP (Maity & Agrawal, 2007). The spectrum of CSNP depicts the characteristic peaks at 676, 617 and 499 cm^{-1} due to the stretching vibration of ZnS molecule (Salavati-Niasari, Ranjbar, & Ghanbari, 2012). It is interesting to note that the characteristic peaks of IONP are not visible in the spectrum of CSNP (Fig. 2d). This is due to the formation of core–shell structures with high deposition of ZnS on the surface of IONP.

3.3. XRD analysis

XRD pattern of the IONP (Fig. 3a) shows the phases such as (2 2 0), (3 1 1), (4 0 0), (4 2 2), (5 1 1) and (4 4 0). The position of the entire indexed diffraction peaks matches well with that of Fe_3O_4 (JCPDS No. 85-1436). Fig. 3b shows the XRD pattern of CSNP, which depicts new phases such as (1 1 1) and (2 2 0), apart from the phases of Fe_3O_4. These new phases indexed in the CSNP indicate the presence of cubic zinc blende structure of ZnS, which matches well with the standard (JCPDS No. 05-566). These results indicate that the ZnS is well-crystallized and coated around the surface of the IONP (Salavati-Niasari et al., 2012; Weesiong et al., 2010; Yu, Ji, Wang, Sun, & Du, 2010).

3.4. EDX analysis

Fig. 4 shows the EDX spectrum of IONP and CSNP. EDX spectrum of IONP show the presence of iron and oxygen at 75.2 and 23 wt.%, respectively (Fig. 4a). The presence of sulphur and

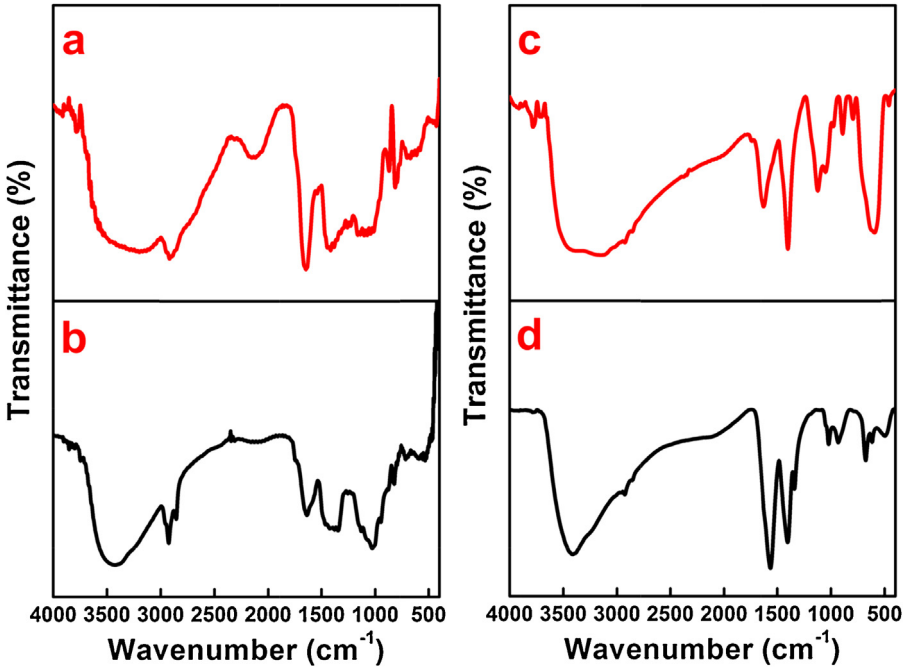

Fig. 2. FTIR Spectrum of (a) GG, (b) AGG, (c) IONP and (d) CSNP.

chlorine elements in traces is also noted in the prepared IONP, which may be due to the unreacted $FeCl_3$ and $FeSO_4$. On the other hand, the CSNP show the presence of zinc, sulphur, iron and oxygen at 37.4, 10.5, 21.2 and 30.9 wt.%, respectively (Fig. 4b). These results substantiate the formation of CSNP with ZnS shells around the core of IONP.

3.5. VSM analysis

The magnetization curves of the IONP and CSNP are shown in Fig. 4c. The saturation magnetization of IONP is 58.69 emu/g at room temperature with 0 Oe coercivity demonstrating the ferromagnetic behavior. However, the saturation magnetization of CSNP is only 3.06 emu/g. The reduction in magnetic properties is due to the formation of core–shell structure over the surface of the IONP. It is known that ZnS is a diamagnetic II–VI semiconductor and hence the coating of ZnS on IONP is expected to reduce the magnetic properties.

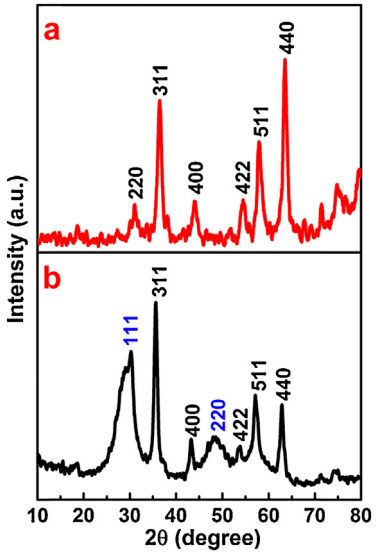

Fig. 3. XRD patterns of as-synthesized (a) IONP and (b) CSNP.

3.6. Electron microscopic studies

High resolution scanning electron microscopic images showing the surface morphology of the synthesized IONP and CSNP are given in Fig. 5. The SEM micrographs of the IONP show that the average particle size is 16 ± 1.5 nm and the particles are spherical (Fig. 5a). On the other hand, the morphology of CSNP is not clear due to the excessive deposition of ZnS on the surface of IONP leading to aggregation (Fig. 5b). High resolution transmission electron microscopic image of CSNP shows aggregated core–shell nanoparticles with spherical shape (Fig. 5c). The average particle size is estimated as 25 ± 4 nm. The presence of dark iron oxide spherical nanoparticles surrounded by lighter ZnS confirms the formation of core–shell nanoparticles.

3.7. Effect of temperature and pH

The aminated GG attains a strong gel structure by interpenetrating polymeric networking without using any toxic crosslinking agents. The digital photographs of AGG, AGG-CSNP and AGG-CSNP-DOX hydrogel systems at 27 and 37 °C are shown in Fig. 6a and b, respectively. When the AGG solution is sonicated and heated at 37 °C, the gelation occurs and hydrogel forms. However, it does not form hydrogel at 0, 5 and 27 °C. It is also observed that the formed hydrogel systems show remarkably high stability up to 95 °C. Also, the hydrogel systems do not show any significant change in their structure at different pH conditions (pH 2–12). The results revealed that the prepared injectable hydrogel system is highly stable when compared to various other hydrogel systems reported based on synthetic polymers and toxic cross linking agents (Kim et al., 2012; Tan et al., 2012). Hence, it is possible to use the prepared thermo-responsive and thermo-stable hydrogel system for solid tumor treatment applications such as hyperthermia.

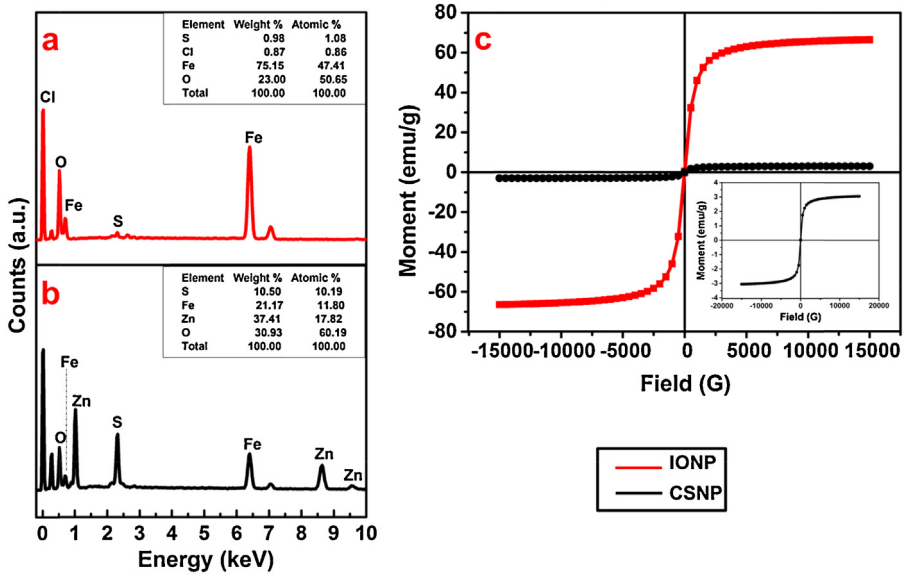

Fig. 4. EDX spectrum of (a) IONP and (b) CSNP; (c) magnetization curves of IONP and CSNP analyzed using VSM. Inset shows the magnetization curve of CSNP showing the ferromagnetic behavior.

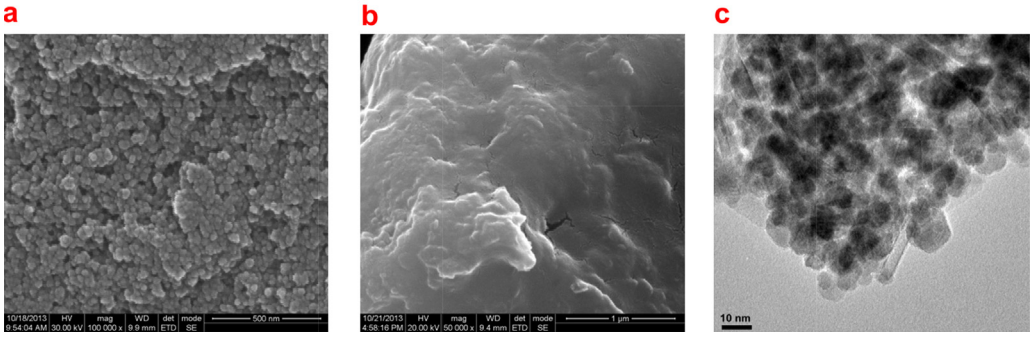

Fig. 5. High resolution scanning electron microscopic images showing the morphology of (a) IONP and (b) CSNP; (c) high resolution transmission electron microscopic image showing the morphology of CSNP.

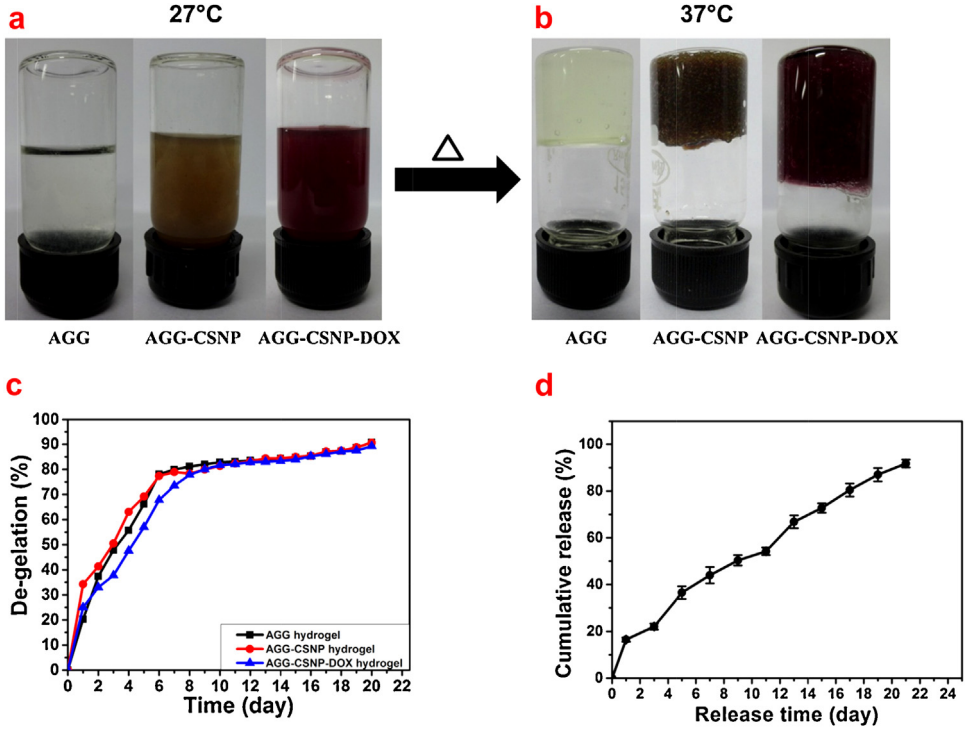

Fig. 6. Digital images showing the physical state of AGG, AGG-CSNP and AGG-CSNP-DOX systems as a function of temperature at (a) 27 °C and (b) 37 °C; (c) in vitro de-gelation patterns of AGG, AGG-CSNP and AGG-CSNP-DOX hydrogel systems; (d) in vitro drug release pattern of AGG-CSNP-DOX hydrogel.

3.8. In vitro hydrogel stability and drug release studies

The injectable biodegradable hydrogel can offer a long-term theranostic and drug release to the infection site within the tumor tissues. Recently, it evolved as a direct treatment for the tumor tissues by preventing the side effects and providing long term diagnosis to the patients (Al-Abd, Hong, Song, & Kuh, 2010; Chun et al., 2009). Hence, the de-gelation studies are important to understand the stability of the hydrogel during the tumor treatment process. The in vitro de-gelation studies of the AGG, AGG-CSNP and AGG-CSNP-DOX hydrogel systems are shown in Fig. 6c. It is seen that the maximum de-gelation for all the AGG, AGG-CSNP and AGG-CSNP-DOX hydrogel systems is around 90% after 20 day incubation. It is important to note that the AGG, AGG-CSNP and AGG-CSNP-DOX hydrogel systems do not show any significant difference in the de-gelation rate. This implies that the CSNP and DOX materials have evenly dispersed and interlaced in the interpenetrating polymeric network of the AGG hydrogel system. The results confirm that the CSNP and DOX do not alter the hydrogel system and provide long term stability, drug delivery and theranostic properties for the solid tumor treatment.

Fig. 6d shows the release of DOX from AGG-CSNP-DOX hydrogel system determined using UV-visible spectrophotometer. A progressive linear release pattern of DOX is seen from 0th day up to 21st day of incubation demonstrating the sustained drug delivery. It is seen that the mean cumulative amount of DOX released was up to 92% after 21st day of incubation. It should be noted that the long term DOX release was primarily due to the strong interlacing of DOX within the aminated GG polymeric network chains. It is seen that the de-gelation rate is directly proportional to the rate of DOX release from the hydrogel. Hence, the results show a sustained CSNP and DOX release from the hydrogel. Hence, the results suggest that the prepared hydrogel can be used directly for drug delivery, hyperthermia and theranostic applications.

4. Conclusions

A stable injectable magnetic nanoparticle incorporated hydrogel system was prepared as an alternative for the long-term drug release and diagnosis to the cancer patients. The injectable hydrogel system consisted of AGG as the biodegradable polymer and gelling agent, DOX as the anticancer drug and CSNP as the imaging agent without using any toxic crosslinkers. Studies reveal that a strong gel was formed by the reaction between NH_3^+ groups and water molecules at 37 °C and stable over a wide temperature and pH range. The in vitro drug releasing tendency of DOX is seen up to 21st day of incubation demonstrating the sustained delivery over long period. Hence, the prepared thermoresponsive injectable hydrogel system has promising applications such as sustained drug release, hyperthermia and theranostic for the solid tumor treatment.

Acknowledgements

Authors thank SERC, Department of Science and Technology, India for providing financial assistance under the Fast Track Scheme for Young Scientists (SERC/ET-0359/2011). We also thank SAIF, IIT Madras for providing the VSM and SEM facility. CSIR-CLRI Communication No. is 1045.

References

Al-Abd, A. M., Hong, K. Y., Song, S. C., & Kuh, H. J. (2010). Pharmacokinetics of doxorubicin after intratumoral injection using a thermosensitive hydrogel in tumor-bearing mice. *Journal of Controlled Release*, *142*, 101–107.

Arola, O. J., Saraste, A., Pulkki, K., Kallajoki, M., Parvinen, M., & Voipio-Pulkki, L. M. (2000). Acute doxorubicin cardiotoxicity involves cardiomyocyte apoptosis. *Cancer Research*, *60*, 1789–1792.

Bajpai, S. K., Saxena, S. K., & Sharma, S. (2006). Swelling behavior of barium ions-crosslinked bipolymeric sodium alginate-carboxymethyl guar gum blend beads. *Reactive and Functional Polymers*, *66*, 659–666.

Bubnis, W. A., & Ofner, C. M., III. (1992). The determination of ∈-amino groups in soluble and poorly soluble proteinaceous materials by a spectrophotometric method using trinitrobenzenesulfonic acid. *Analytical Biochemistry*, *207*, 129–133.

Burke, M. D., Park, J. O., Srinivasarao, M., & Khan, S. A. (2000). Diffusion of macromolecules in polymer solutions and gels: A laser scanning confocal microscopy study. *Macromolecules*, *33*, 7500–7507.

Burruano, B. T., Schnaare, R. L., & Malamud, D. (2002). Synthetic cervical mucus formulation. *Contraception*, *66*, 137–140.

Chang, C., & Zhang, L. (2011). Cellulose-based hydrogels: Present status and application prospects. *Carbohydrate Polymers*, *84*, 40–53.

Chourasia, M., & Jain, S. (2004). Polysaccharides for colon targeted drug delivery. *Drug Delivery*, *11*, 129–148.

Chun, C. J., Lee, S. M., Kim, C. W., Hong, K. Y., Kim, S. Y., Yang, H. K., et al. (2009). Doxorubicin-polyphosphazene conjugate hydrogels for locally controlled delivery of cancer therapeutics. *Biomaterials*, *30*, 4752–4762.

Corot, C., Robert, P., Idee, J. M., & Port, M. (2006). Recent advances in iron oxide nanocrystal technology for medical imaging. *Advanced Drug Delivery Reviews*, *58*, 1471–1504.

Gelperina, S., Khalansky, A., Skidan, I., Smirnova, Z., Bobruskin, A., Severin, S., et al. (2002). Toxicological studies of doxorubicin bound to polysorbate 80-coated poly (butyl cyanoacrylate) nanoparticles in healthy rats and rats with intracranial glioblastoma. *Toxicology Letters*, *126*, 131–141.

Gliko-Kabir, I., Yagen, B., Baluom, M., & Rubinstein, A. (2000). Phosphated crosslinked guar for colon-specific drug delivery: II in vitro and in vivo evaluation in the rat. *Journal of Controlled Release*, *63*, 129–134.

Gupta, A. K., & Gupta, M. (2005). Synthesis and surface engineering of iron oxide nanoparticles for biomedical applications. *Biomaterials*, *26*, 3995–4021.

Gupta, A. K., Naregalkar, R. R., Vaidya, V. D., & Gupta, M. (2007). Recent advances on surface engineering of magnetic iron oxide nanoparticles and their biomedical applications. *Nanomedicine: Nanotechnology, Biology, and Medicine*, *2*, 23–39.

Huang, Y., Lu, J., & Xiao, C. (2007). Thermal and mechanical properties of cationic guar gum/poly(acrylic acid) hydrogel membranes. *Polymer Degradation and Stability*, *92*, 1072–1081.

Kim, J. I., Lee, B. S., Chun, C., Cho, J. K., Kim, S. Y., & Song, S. C. (2012). Long-term theranostic hydrogel system for solid tumors. *Biomaterials*, *33*, 2251–2259.

Kintzel, P. E., & Dorr, R. T. (1995). Anticancer drug renal toxicity and elimination: Dosing guidelines for altered renal function. *Cancer Treatment Reviews*, *21*, 33–64.

Kulkarni, A. R., Soppimath, K. S., Aminabhavi, T. M., Dave, A. M., & Mehta, M. H. (1999). Urea-formaldehyde crosslinked starch and guar gum matrices for encapsulation of natural liquid pesticide [*Azadirachta indica* A. Juss. (neem) seed oil]: Swelling and release kinetics. *Journal of Applied Polymer Science*, *73*, 2437–2446.

Maity, D., & Agrawal, D. C. (2007). Synthesis of iron oxide nanoparticles under oxidizing environment and their stabilization in aqueous and non-aqueous media. *Journal of Magnetism and Magnetic Materials*, *308*, 46–55.

Mitra, S., Gaur, U., Ghosh, P., & Maitra, A. (2001). Tumour targeted delivery of encapsulated dextran-doxorubicin conjugate using chitosan nanoparticles as carrier. *Journal of Controlled Release*, *74*, 317–323.

Narasimha Murthy, S., Hiremath, S. R. R., & Paranjothy, K. (2004). Evaluation of carboxymethyl guar films for the formulation of transdermal therapeutic systems. *International Journal of Pharmaceutics*, *272*, 11–18.

Salavati-Niasari, M., Ranjbar, M., & Ghanbari, D. (2012). A rapid microwave route for the synthesis of ZnS nanoparticles. *Journal of Nanostructures*, *1*, 231–235.

Santra, S., Tapec, R., Theodoropoulou, N., Dobson, J., Hebard, A., & Tan, W. (2001). Synthesis and characterization of silica-coated iron oxide nanoparticles in microemulsion: The effect of nonionic surfactants. *Langmuir*, *17*, 2900–2906.

Simi, C. K., & Abraham, T. E. (2010). Physico chemical properties of aminated tamarind xyloglucan. *Colloids and Surfaces B: Biointerfaces*, *81*, 513–520.

Soppirnath, K. S., & Aminabhavi, T. M. (2002). Water transport and drug release study from cross-linked polyacrylamide grafted guar gum hydrogel microspheres for the controlled release application. *European Journal of Pharmaceutics and Biopharmaceutics*, *53*, 87–98.

Tan, R., She, Z., Wang, M., Fang, Z., Liu, Y., & Feng, Q. (2012). Thermo-sensitive alginate-based injectable hydrogel for tissue engineering. *Carbohydrate Polymers*, *87*, 1515–1521.

Tayal, A., Pai, V. B., & Khan, S. A. (1999). Rheology and microstructural changes during enzymatic degradation of a guar-borax hydrogel. *Macromolecules*, *32*, 5567–5574.

Von Hoff, D. D., Layard, M. W., Basa, P., Davis, H. L., Von Hoff, A. L., Rozencweig, M., et al. (1979). Risk factors for doxorubicin-induced congestive heart failure. *Annals of Internal Medicine*, *91*, 710–717.

Weesiong, C., Poisim, K., Michael, C., Dino, I., Hongngee, L., Thiankhoon, T., et al. (2010). Heterogeneous seeded growth: Synthesis and characterization of bifunctional Fe_3O_4/ZnO core/shell nanocrystals. *Journal of Physical Chemistry C*, *114*, 8212–8218.

Wong, H. L., Rauth, A. M., Bendayan, R., Manias, J. L., Ramaswamy, M., Liu, Z., et al. (2006). A new polymer–lipid hybrid nanoparticle system increases cytotoxicity of doxorubicin against multidrug-resistant human breast cancer cells. *Pharmaceutical Research*, *23*, 1574–1585.

Yoo, H. S., Lee, K. H., Oh, J. E., & Park, T. G. (2000). In vitro and in vivo anti-tumor activities of nanoparticles based on doxorubicin-PLGA conjugates. *Journal of Controlled Release*, *68*, 419–431.

Yu, X. L., Ji, H. M., Wang, H. L., Sun, J., & Du, X. W. (2010). Synthesis and sensing properties of ZnO/ZnS nanocages. *Nanoscale Research Letters*, *5*, 644–648.